Bienzyme-locked activatable fluorescence probe for specific imaging of tumor-associated mast cells

Yuxuan Hu[a], Jie Yu[a], Mengke Xu[a], and Kanyi Pu[ab]*

AUTHOR ADDRESS

[a]School of Chemistry, Chemical Engineering and Biotechnology, Nanyang Technological University, 70 Nanyang Drive, Singapore 637457, Singapore

[b]Lee Kong Chian School of Medicine, Nanyang Technological University, 59 Nanyang Drive, Singapore 636921, Singapore

*Email: kypu@ntu.edu.sg

ABSTRACT: Tumor-associated mast cells (TAMCs) have been recently revealed to play a multifaceted role in tumor microenvironment. Non-invasive optical imaging of TAMCs is thus highly desired to gain insight into their functions in cancer immunotherapy. However, due to the lack of a single enzyme that is specific to mast cells, common probe design approach based on single enzyme activation is not applicable. Herein, we reported a bienzyme-locked molecular probe (THC_{MC}) based on a photo-induced electron transfer (PET) - intramolecular charge transfer (ICT) hybrid strategy for in vivo imaging of TAMCs. The bienzyme-locked activation mechanism ensures that THC_{MC} exclusively turns on near-infrared (NIR) fluorescence only in the presence of both tryptase and chymase specifically co-expressed by mast cells. Thus, THC_{MC} effectively distinguishes mast cells from other leukocytes including T cells, neutrophils, and macrophages, a capability lacking in single-locked probes. Such a high specificity of THC_{MC} allows to noninvasively track the fluctuation of TAMCs in the tumor of living mice during cancer immunotherapy. The results reveal that the decreased intratumoral signal of THC_{MC} after combination immunotherapy correlates well with the reduced population of TAMCs, accurately predicting the inhibition of tumor growth. Thus, this study not only presents the first NIR fluorescence probe specific for TAMCs, but also proposes a generic bienzyme-locked probe design approach for in vivo cell imaging.

■ INTRODUCTION

Optical imaging provides real-time and non-invasive approaches for monitoring biomolecules of interest within living systems, showing significant promise for biomedical research and clinical diagnosis.[1-4] Compared with "always-on" optical agents, activatable optical probes that produce fluorescence or chemiluminescence exclusively upon interaction with the biomarkers of interest have enhanced signal-to-background ratios and lowered detection limits, permitting specific and sensitive detection and tracking biological and pathological processes in a variety of diseases.[5-8] However, most of them turn on their optical signal upon reaction with one single biomarker, which is termed as the single-locked optical probes. Such design can suffer from "false positive" signals in the complex biological environment because the nonspecific cells or tissues could express certain level of the corresponding biomarker. Therefore, dual-locked activatable optical probes have been recently developed, which have two responsive sites and only turn on their signals in the presence of both biomarkers.[9, 10] Due to their high specificity relative to the single-locked counterparts, dual-locked probes enabled specific detection of hepatopathy,[11, 12] and cancer.[13-15]

Currently, there are two major options for the development of dual-locked optical probes for simultaneous detection of two enzymes being dual-quenching and tandem locked approaches, wherein Förster resonance energy transfer (FRET) and intramolecular charge transfer (ICT) inhibition are the respective mechanisms to induce low fluorescence signal at native state (Figure 1).[16] However, the former contains two chromophore quenchers and often possesses a large molecular size, which could impact its in-vitro diffusion and in-vivo biodistribution abilities.[17] Although the latter has a relatively compact structure, it requires enzymes with high peptide sequence selectivity to enable sequential cleavage of two tandem moieties. This limits the choice of enzymes to a few such as monoamine oxidase (MAO),[18] aminopeptidase N (APN)[19, 20,] and gamma-glutamyl transferase (GGT).[21] Thus, the challenge to fully unlock the potential of bienzyme-locked optical probes in biology and medicine lies in the innovation of new design approaches that lead to the probes with both compact structure and biotarget-choice diversity.

The tandem-locked optical probes have been developed for real-time tracking and non-invasive interpretation of the profiles, distribution, and functions of immune cells in tumors during cancer immunotherapy.[22-25] It has been revealed that the immunotherapy efficacy varies with the infiltration of different immune cells and detection of tumor-infiltrated immune cells could be applied for prognostic stratification and targeted therapy.[26, 27] Mast cells, a

prominent subset of tissue-resident immune cells, play a crucial role in allergic and other inflammatory diseases.[28] However, their functions in the modulation of the tumor immune microenvironment have been less understood. Recently, tumor-associated mast cells (TAMCs) are reported to promote tumor proliferation, angiogenesis, and lymphangiogenesis by releasing growth factors and proteolytic enzymes. They are also found to contribute to immune suppression during immune checkpoint therapy through the expression of immunosuppressive programmed cell death protein 1 (PD-1) and programmed death-ligand 1 (PD-L1).[29-31] However, in some other cases, TAMCs were revealed to be associated with tumor suppression.[32] Therefore, to gain insights into the roles of TAMCs during cancer immunotherapy, non-invasive in vivo optical imaging of TAMCs is highly desired, which remains to be exploited.

In this study, we propose a photoinduced electron transfer (PET)-ICT hybrid bienzyme-locked strategy towards a compact bienzyme-locked activatable fluorescent probe (THC_{MC}) for sensitive and specific detection of TAMCs (Figure 1 and 2a). THC_{MC} comprises four key units: an ICT signaling moiety, a tumor-passive targeting moiety, a tryptase-cleavable ICT-inhibiting moiety, and a chymase-cleavable PET-quenching moiety (Figure 2b). Tryptases and chymases are two type of serine proteases specifically co-expressed by mast cell,[33] which are reported to promote angiogenesis and lymphangiogenesis through the activation of protease-activate receptor 2 and matrix metalloproteinase pro-enzymes, or direct degradation of extracellular matrix components.[34] THC_{MC} is initially non-fluorescence as its ICT is inhibited by the caging of the electron-donating hydroxyl group with tryptase-cleavable moiety and the PET process is induced by a miniaturized quencher at the end of the chymase-cleavable moiety. Only the presence of both TAMC biomarkers allows THC_{MC} to release the signaling moiety and turn on the near-infrared (NIR) fluorescence, improving the detection accuracy. Therefore, THC_{MC} can specifically detect TAMCs, while the single-locked probes (HCs) fail to do so.

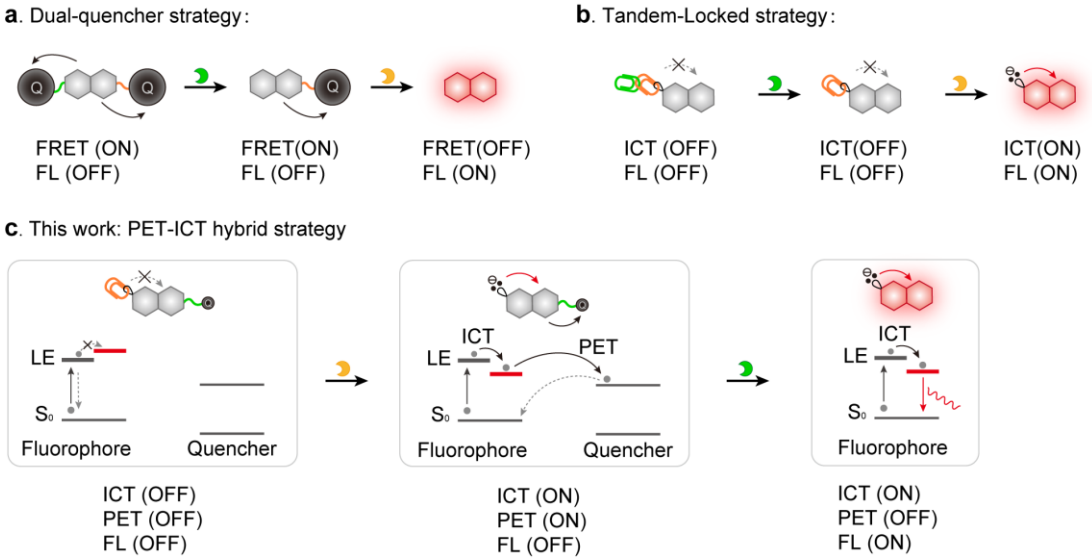

Figure 1. a) Schematic of dual-quencher strategy and two representative quenchers in near-infrared (NIR) region. The fluorescence (FL) is initially quenched by two quenchers via Förster resonance energy transfer (FRET), two proteolytic processing events are required to activate fluorescence. **b**) Schematic of tandem-locked strategy. The intramolecular charge transfer (ICT) is inhibited by a caging group containing two responses, which can only be activated by the correct combination and sequence of triggers. **c**) Schematic of PET-ICT hybrid strategy in this work. The fluorescence is initially quencher via ICT inhibition and further suppressed by photo-induced electron transfer (PET) after trigger-induced ICT recovery. Only the simultaneous removal of ICT inhibitor and PET quencher can activate the NIR fluorescence signal. LE, local excited state.

■ RESULTS AND DISCUSSION

Synthesis and Characterization. To construct THC_{MC}, a three-branch hemi-cyanine fluorophore (THC) scaffold with a benzylamine group on the C5 position of the indole ring was designed and synthesized (Figure S1). First, the hydroxyl group of THC was caged by a tryptase-responsive moiety composed of a self-immolative linker connected to peptide substrate N-tosyl-Gly-Pro-Lys (GPK) specific towards tryptase.[35] Then, the benzylamine group of THC was conjugated with a dinitrobenzene (DNB) fluorescence quencher via chymase-cleavable peptide sequences N-Gly-Leu-Val-Val-Ser-Leu (GLVVSL).[36] The azide group of THC was conjugated to alkyne-functionalized Poly(N-vinyl-2-pyrrolidone)(PVP) chain with molecular weight of 2600 Da to enhance hydrophilicity and tumor-passive accumulation capability.[37] Single-locked probes (HC_{TR} and HC_{CH}) only caged by the tryptase-responsive moiety or only linked with DNB quencher via the chymase-cleavable peptide were also synthesized as the controls. All the intermediates and the final compounds were characterized by proton nuclear magnetic resonance spectra (^{1}H NMR) and electrospray ionization mass spectra (ESI-MS) (Figure S14-S50).

Because of the minimal spectral overlap between DNB and NIR fluorophores, DNB was not often considered as a quencher for fluorophores in NIR region. To determine the feasibility of electron transfer from THC to DNB group, the

density-functional theory (DFT)/ Time-dependent density-functional theory (TD-DFT) calculations were conducted employing the B3LYP method and a 6-31G (d) basis set incorporated in Gaussian 09 software. As shown in Figure 2c, the lowest unoccupied molecular orbital (LUMO) energy level of DNB group (-2.78 eV) lies between the highest occupied molecular orbital (HOMO, -2.21 eV) and LUMO (-4.65 eV) energy level of THC, making the PET process in the excited state from THC to DNB group feasible.[38] To further validate and measure the PET-induced quenching, titration experiment was performed by gradual addition of DNB into the solution of THC, followed by measurement of steady-state fluorescence intensities of THC. The substantial quenching of THC by DNB was observed (Figure S2). Such efficient quenching was also observed when DNB was covalently linked with THC, as exemplified by the nearly nonfluorescent THC-DNB. Moreover, THC-DNB showed fluorescence recovery upon removal of DNB in the presence of chymase, indicating that the DNB quenching strategy was applicable for the design of chymase-activatable fluorescence probe.

In vitro detection. To investigate the in vitro responses of THC_{MC} and HCs, the optical properties were measured in the absence or presence of biomarkers. THC_{MC} initially showed two characteristic absorption peaks at 620 and 675 nm and was non-fluorescent due to ICT inhibition. After incubation with tryptase alone, a new peak at 690 nm corresponding to the unaged THC emerged (Figure 3b), indicating the tryptase-induced cleavage of peptide substrate followed by the spontaneous uncaging of hydroxyl group of THC_{MC}. However, THC_{MC} remained nonfluorescent owing to the PET quenching by DNB group. After incubation with chymase alone, THC_{MC} showed no absorption and fluorescence changes due to the presence of ICT inhibition. Only after incubation with both enzymes, the NIR fluorescence of THC_{MC} was turned on, showing an 18-fold increase compared to that before enzyme incubation (Figure 3c and 3d). In contrast, HC_{TR} and HC_{CH} showed 20- and 22-fold fluorescence enhancement after incubation with tryptase and chymase, respectively (Figure S3 and S4). Moreover, the fluorescence signal of THC_{MC} showed negligible increase after incubation with other interfering enzymes (Figure 3e and S5), confirming its high specificity.

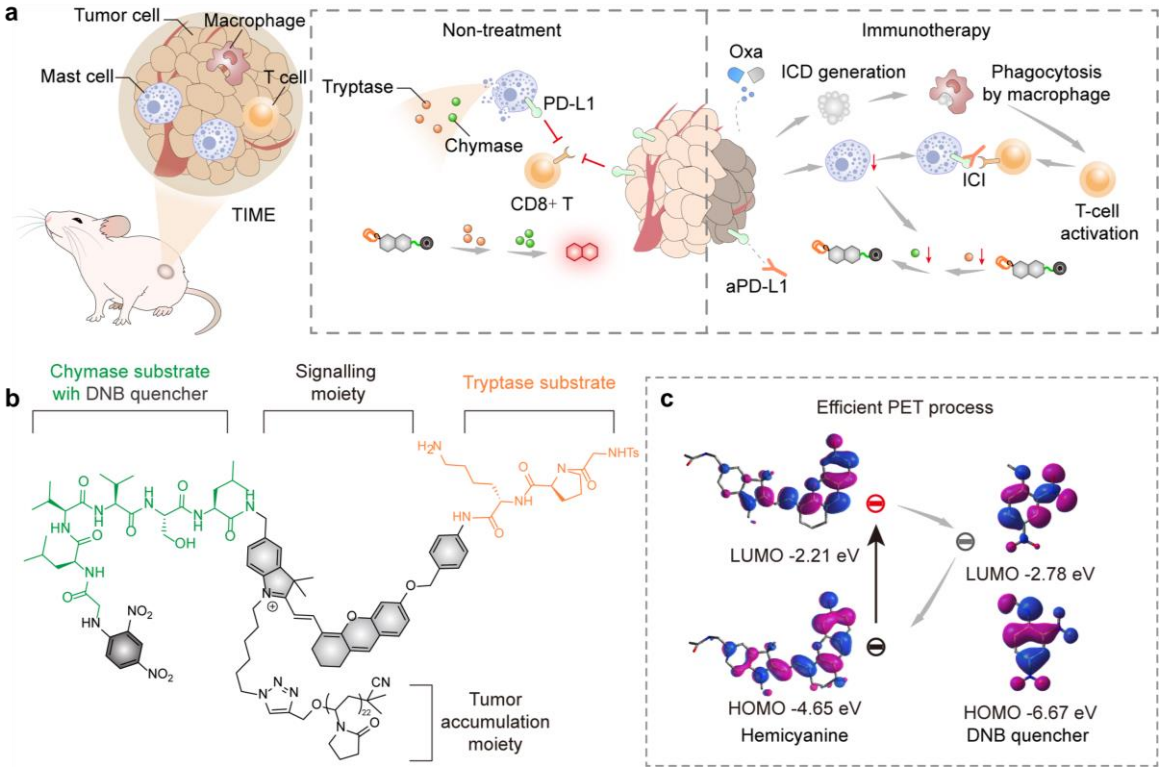

Figure 2. a) Molecular mechanism of bienzyme-locked molecular probe (THC_{MC}) for real-time imaging of tumor-associated mast cells (TAMCs) during cancer immunotherapy. **b**) Chemical structures of THC_{MC}. **c**) HOMO, and LUMO of three-branch hemi-cyanine fluorophore (THC) and dinitrobenzene (DNB) group as calculated via density functional theory (DFT) calculations and proposed mechanism of the photoinduced electron transfer (PET) from THC to DNB.

High-performance liquid chromatography (HPLC) analysis was applied to investigate the structural changes and the enzymatic kinetics of THC_{MC} precursor ($THCP_{MC}$, without PVP) in response to the biomarkers. $THCP_{MC}$ instead of THC_{MC} was used for HPLC study because the PVP of THC_{MC} dominated its elution property and no obvious change in its HPLC trace could be detected after enzyme cleavage. As shown in the HPLC profile, incubation of $THCP_{MC}$ with both tryptase and chymase generated a new peak (t_R = 7.0 min) corresponding to the activated $THCP_{MC}$, which was undetectable upon incubation with tryptase or chymase alone. The enzymatic Michaelis-Menten constant (K_m), catalytic

rate constants (k_{cat}), and catalytic efficiency (k_{cat}/K_m) of tryptase toward $THCP_{MC}$ were determined to be 42.8 μM and 7.45 min^{-1} and 0.003 $\mu M^{-1}s^{-1}$, respectively. Similarly, the K_m, $k_{cat,}$ and k_{cat}/K_m of chymase toward $THCP_{MC}$ were calculated to be 67.7 μM, 3.77 min^{-1} and 0.001 $\mu M^{-1}\ s^{-1}$, respectively (Figure 3f).

The capability of THC_{MC} to detect mast cells was tested in a range of living murine cell lines: 4T1 tumor cell line, bone marrow-derived macrophages (BMDMs), primary $CD8^+$ T cells, primary neutrophils, and bone marrow-derived mast cells. Note that all the probes showed negligible cytotoxicity after incubation with 4T1 and mast cells for 24 h (Figure S6). When mast cells were incubated with THC_{MC}, gradually enhanced fluorescence was observed (Figure S7), which colocalized well with the lysosomal tracker (Figure S8). THC_{MC} showed 40- to 50-fold higher signal in mast cells compared to those in other immune cells and 4T1 cells (Figure 4b), suggesting the high specificity of THC_{MC} towards mast cells (Figure 4c). In contrast, HC_{TR} turned on its fluorescence for all cells except for neutrophils, the fluorescence signal in mast cells was 1.8-fold higher than that of THC_{MC}. This could be attributable to the fact that the expression level of tryptase (mMCP-6) is about 3-7-fold higher than that of Chymase (mMCP-5) in the mast cell generated from Balb/c mice.[39] HC_{CH} turned on its NIR fluorescence in neutrophils, which was 1.4-fold and more than 30-fold higher than mast cells and other cell lines, respectively. When neutrophil was pretreated with elastase inhibitor, reduced fluorescence enhancement was observed (Figure S9), suggesting that the fluorescence enhancement of HC_{CH} in neutrophil was attributed to the elastase-like activity of the mouse chymase (mouse mast cell protease 5).[40]

To further confirm that THC_{MC} was activated by the tryptase and chymase together in mast cells, cells were pre-incubated with tryptase inhibitor (Nafamostat mesylate) or chymase inhibitor (Sivelestat). Following treatment with either inhibitor alone, the fluorescence enhancement folds of activated THC_{MC} were 6.9- and 5.6-times lower compared with the untreated group, respectively. In contrast, reduced fluorescence enhancement was only observed in the presence of tryptase inhibitor for HC_{TR} and chymase inhibitor for HC_{CH}, respectively. These results further proved that the bienzyme-locked activation of THC_{MC} by tryptase and chymase, ensuring its high specificity to detect mast cells in the tumor microenvironment.

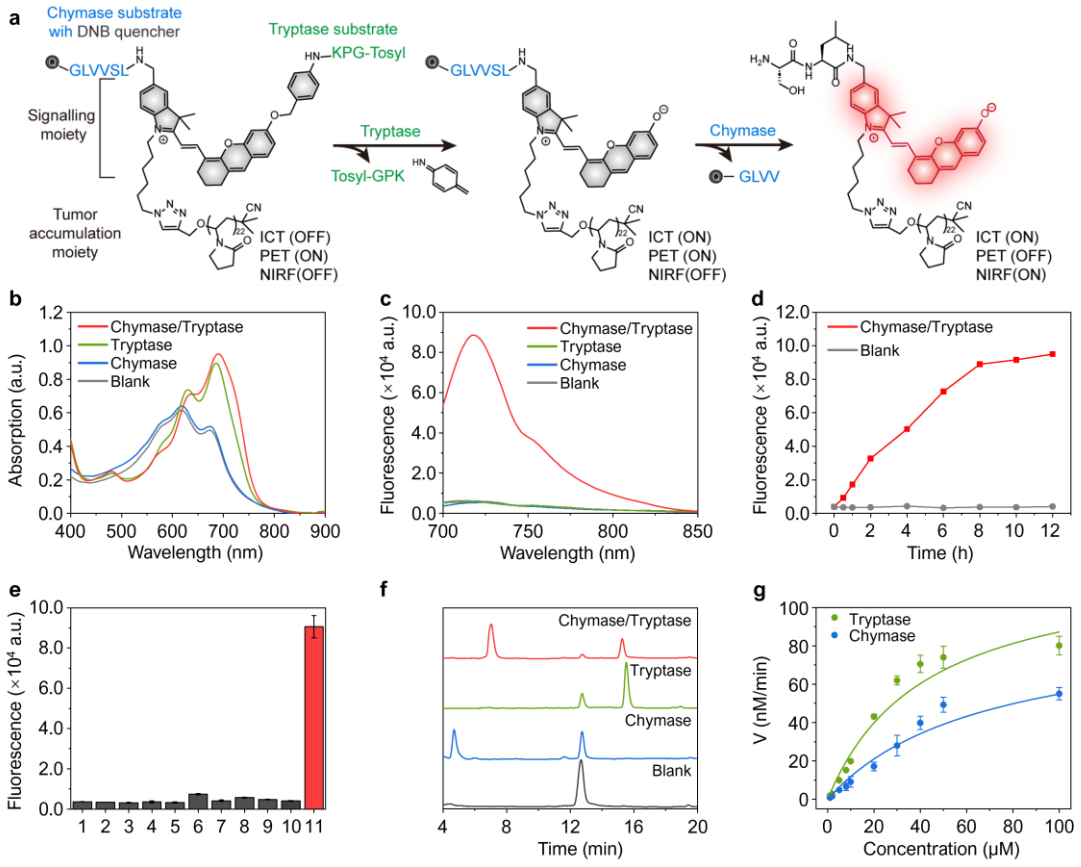

Figure 3. In vitro characterization of THC_{MC}. **a**) Activation mechanism of bienzyme-locked molecular probe (THC_{MC}) for mast cell detection. **b**) UV/Vis absorption spectra and **c**) fluorescence spectra of THC_{MC} (5 μM) after incubation with/without tryptase, chymase, or tryptase & chymase at 37 °C in the PBS buffer (pH 7.4). λ_{ex}=680 nm. **d**) Time-dependent NIR fluorescence enhancement of THC_{MC} after incubation with/without tryptase & chymase at 37 °C in the PBS buffer (pH 7.4). λ_{ex}=680 nm. λ_{em}=720 nm. **e**) NIR fluorescence signals (720 nm) of THC_{MC} after incubation with indicated enzymes in respective buffers at 37 °C for 8 h. Data are presented as mean ± s.d. *n* = 3. **f**) HPLC trace of $THCP_{MC}$ (5 μM) after incubation with/without tryptase, chymase, or tryptase & chymase at 37 °C in the PBS buffer (pH 7.4) for 8 h. **g**) Nonlinear regression analysis of cleavage rate V of $THCP_{MC}$ by tryptase and chymase as a function of substrate concentration. 1: Blank; 2: cathepsin B; 3: alanine

aminopeptidase; 4: caspase-1; 5: caspase-3; 6: Gamma-glutamyltransferase; 7: trypsin; 8: neutrophil elastase; 9: chymase; 10: tryptase; 11: tryptase&chymase.

In vivo detection of TAMCs in tumor-bearing mice. The ability of THC_{MC} for in vivo detection of TAMCs during tumor immunotherapy was investigated in 4T1 tumor-bearing mice. 4T1 tumor is known to be poorly immunogenic, and recently was found to have infiltrated mast cells.[41] Tumor-bearing mice were administered a combination of anti-programmed death-ligand 1 (aPD-L1) and oxaliplatin (Oxa) (aPD-L1/Oxa), tryptase inhibitor (nafamostat mesylate, intratumoral injection), or saline (Figure 5a). After treatment, THC_{MC} was intravenously injected into the living mice for the longitudinal NIR fluorescence imaging for 72 h, and the signals at the tumor region were quantified (Figure 5a and 5b). For all groups, the NIR fluorescence signals in the tumor regions gradually increased and reached maxima at 12 h post-injection, followed by slow decrease in the rest of imaging course (Figure 5b and S10). Quantification showed that the maximal tumor NIR fluorescence for the immunotherapy group was 1.6-fold lower than that for the saline-treated mice, but 1.3-fold higher than the inhibitor-treated group. This proved the reduced amount of activated THC_{MC} after immunotherapy and specific activation of THC_{MC} by intratumoral tryptase.

To determine if the intratumoral signal of THC_{MC} was related to the infiltration level of TAMCs, flow cytometry and immunofluorescence staining were conducted for the tumor tissues from different treatment groups (Figure S11). As shown in Figure 5d, the amount of TAMCs ($C\text{-}kit^{+}Fc\varepsilon RI^{+}$) for the immunotherapy group was 2.4-fold less than those for the saline and inhibitor-treated groups. This was positively correlated with the intratumoral signal of THC_{MC}. Immunofluorescence staining further showed that the NIR fluorescence signals from THC_{MC} had good colocalization with pseudo-green signals from FcεRI staining (Figure 5g). These data confirmed the capability of THC_{MC} for non-invasive and real-time profiling TAMCs in 4T1 tumors.

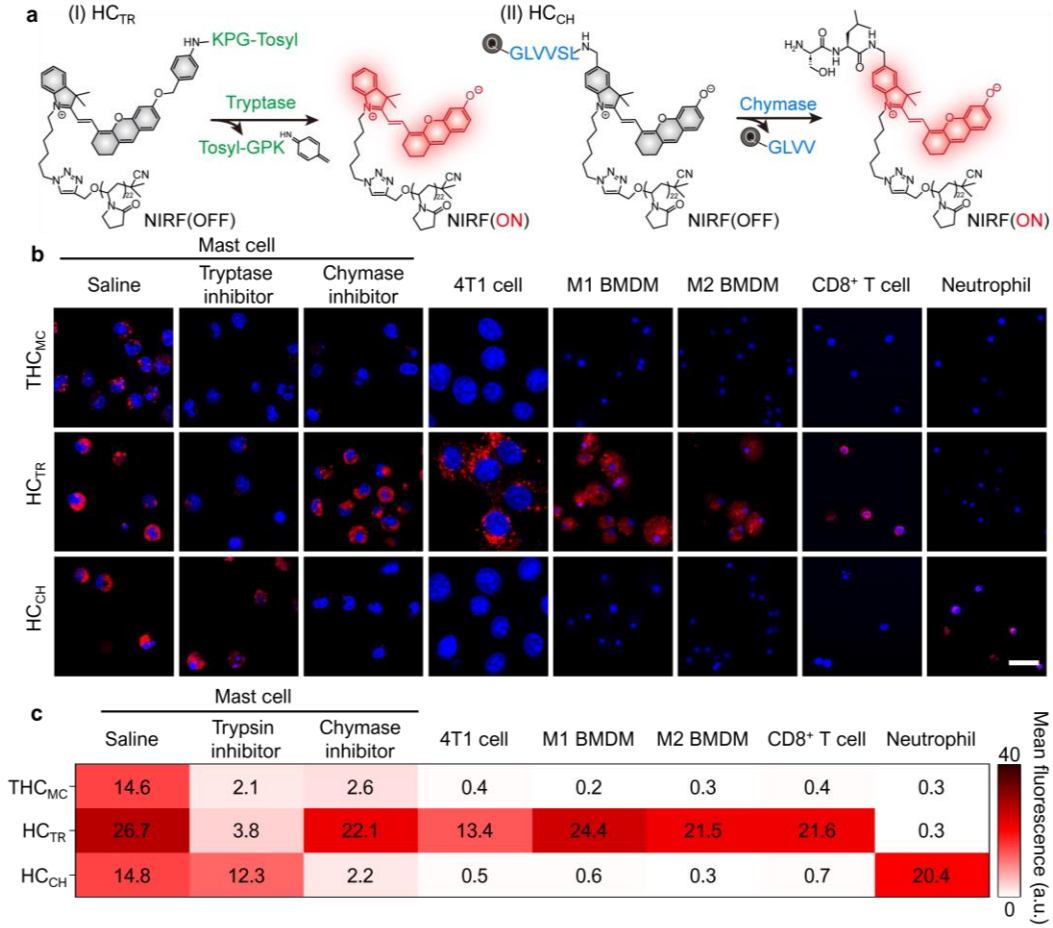

Figure 4. In vitro imaging of THC_{MC}, HC_{TR}, and HC_{CH} in living cells. **a**) Activation mechanism of single-locked molecular probes (HCs). **b**) Confocal images of 4T1 tumor cell line, bone marrow-derived macrophages (BMDM), primary $CD8^{+}$ T cells, primary neutrophils, and bone marrow-derived mast cells. Cells were pre-treated with or without tryptase inhibitor (Nafamostat mesylate, 20 μM, 1 h), chymase inhibitor (Sivelestat, 20 μM, 1 h), then incubated with THC_{MC}, HC_{TR}, and HC_{CH} for real-time imaging. The experiments were repeated three times, with similar results. Scale bar: 10 μm. **c**) The quantified mean fluorescence values in Figure 3**b**.

To validate the capability of THC_{MC} for prediction of the therapeutic outcomes, the relative tumor volumes of each group were continuously monitored for 20 days (Figure S12). A positive correlation between the intratumoral signal of THC_{MC} on day 6 and the relative tumor volumes on day 20 was observed with a Pearson's correlation coefficient (P) of 0.98 (Figure 5f). Considering that the fluorescence imaging was performed on day 6, which was two weeks earlier than the treatment endpoint, THC_{MC} could serve as a noninvasive and accurate tool to predict therapeutic outcomes. Moreover, THC_{MC} could be applied for the microscopic examination of whole-tumor sections. As shown in Figure S13, high densities of active THC_{MC} were observed to diffuse to the center for saline-treated sections, which was 2.4-fold lower after PD-L1/Oxa treatment. This suggested the reduced infiltration of TAMCs after combined immunotherapy.

■ CONCLUSION

In summary, we have developed a bienzyme-locked activatable molecular fluorescent probe (THC_{MC}) based on PET-ICT hybrid strategy for non-invasive and real-time monitoring of TAMCs during immunotherapy. Using the three-branch hemi-cyanine fluorophore (THC) scaffold, THC_{MC} incorporated tryptase-cleavable ICT-inhibiting moiety and chymase-cleavable PET-quenching moiety, ensuring specific fluorescence turn-on only in the present of both tryptase and chymase specifically co-expressed by mast cells. The in vitro results revealed that THC_{MC} was specifically activated only upon interaction with both tryptase and chymase and an 18-fold fluorescence enhancement was observed. Such a high specificity allowed THC_{MC} to distinguish mast cells from other leukocytes including T cells, neutrophils, and macrophages, while single-locked probes failed to do so. The presence of PVP endowed THC_{MC} with passive tumor accumulation, enabling noninvasive monitoring of the fluctuation of TAMCs in the tumor of living mice during cancer immunotherapy. The results revealed that the intratumoral fluorescence signal from THC_{MC} was correlated with the infiltration of TAMCs in tumors and a 1.6-fold reduction was observed after combination immunotherapy, which was confirmed by flow cytometry and immunofluorescence staining.

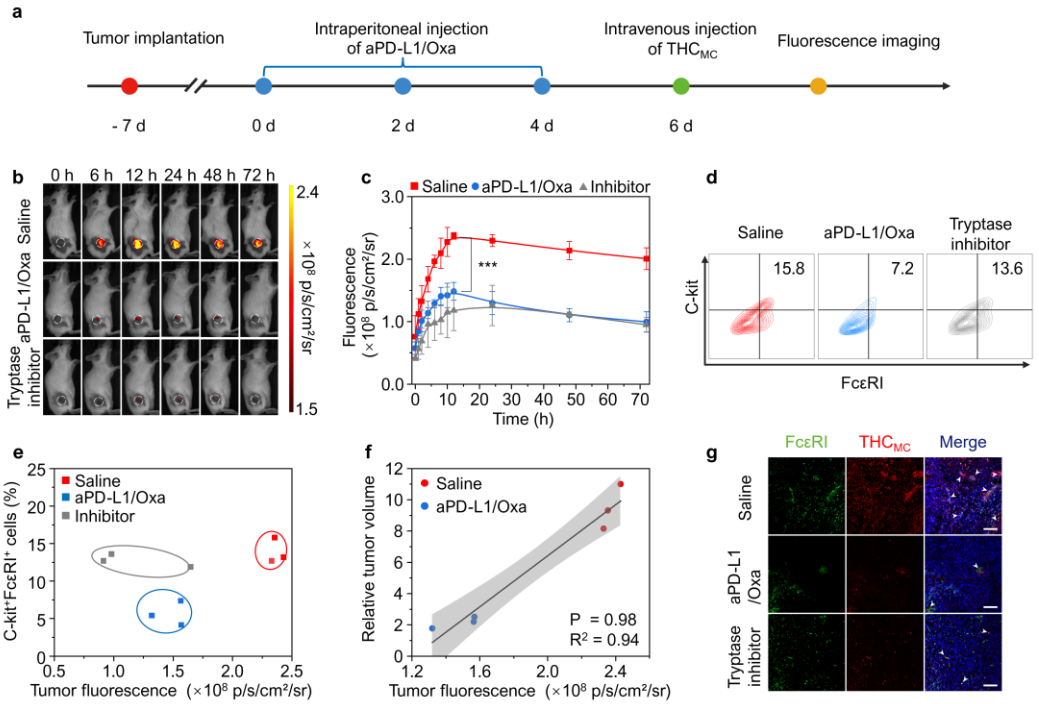

Figure 5. Real-time imaging of TAMCs in living mice. **a**) Schematic illustration of therapy and real-time imaging of TAMCs. **b**) Real-time imaging of 4T1 tumor-bearing mice with different treatments after intravenous injection of THC_{MC} (5 μmol kg^{-1}). NIRF images were acquired at emission of 720 nm upon excitation at 675 nm. **c**) Fluorescence intensity at tumor sites as a function of post-injection time points of probes. Data are presented as mean ± s.d., n = 3. *** for $p < 0.001$. **d**) Flow cytometry assay of C-kit$^+$FcεRI$^+$ TAMCs gated by CD45$^+$ cells in the tumors of mice with different treatments. **e**) Correlation between C-kit$^+$FcεRI$^+$ TAMCs (%) and tumor radiance (10^8 p/s/cm^2/sr). **f**) Correlation between relative tumor volume and tumor radiance (10^8 p/s/cm^2/sr). *P*: Pearson's correlation coefficient, R^2: coefficient of determination. **g**) Representative confocal fluorescence microscopy images of tumor slices from mice with different treatments at 72 h post-injection of THC_{MC}. White arrows indicate the overlap of fluorescence signals from TMC_{MC} and FcεRI staining. Scale bar = 100 μm.

To the best of our knowledge, THC_{MC} is the first optical probe capable of noninvasive and real-time in vivo tracking of mast cells. It can serve as a useful tool to gain insight into the function of mast cells in tumor microenvironment. Furthermore, the PET-ICT hybrid dual-lock strategy is more promising than the dual-quenching and tandem-locked strategies to develop bienzyme-locked activatable probes as it integrates the advantages of biotarget-choice diversity and structural compact. By simply changing the enzyme-responsive moieties, this hybrid strategy can be generalized

for the detection of multiple enzymes in pathophysiological processes with improved specificity and accuracy for biomedical research and clinical diagnosis.

ASSOCIATED CONTENT

Supporting Information

The Supporting Information is available free of charge on the ACS Publications website.

Detailed experimental procedures and supporting figures as described in the text (PDF)

AUTHOR INFORMATION

Corresponding Author

* **Kanyi Pu** - School of Chemistry, Chemical Engineering and Biotechnology, Nanyang Technological University, Singapore 637457; Lee Kong Chian School of Medicine, Nanyang Technological University, Singapore 636921; https://orcid.org/0000-0002-8064-6009; Email: kypu@ntu.edu.sg

ACKNOWLEDGMENT

K.P. thanks Singapore National Research Foundation (NRF) (NRF-NRFI07-2021-0005) and the Singapore Ministry of Education Academic Research Fund Tier 2 (MOE-T2EP30220-0010, MOE-T2EP30221-0004) for financial support. Animal experiments were performed in compliance with the Guidelines for Care and Use of Laboratory Animals of the Nanyang Technological University-Institutional Animal Care and Use Committee (NTU-IACUC) and approved by the Institutional Animal Care and Use Committee (IACUC) for Animal Experiments, Singapore.

REFERENCES

(1) Razgulin, A.; Ma, N.; Rao, J., Strategies for in vivo imaging of enzyme activity: an overview and recent advances. *Chem. Soc. Rev.* **2011,** *40*, 4186-4216.

(2) Zeng, S.; Liu, X.; Kafuti, Y. S.; Kim, H.; Wang, J.; Peng, X.; Li, H.; Yoon, J., Fluorescent dyes based on rhodamine derivatives for bioimaging and therapeutics: recent progress, challenges, and prospects. *Chem. Soc. Rev.* **2023,** *52*, 5607-5651.

(3) Han, H. H.; Tian, H.; Zang, Y.; Sedgwick, A. C.; Li, J.; Sessler, J. L.; He, X. P.; James, T. D., Small-molecule fluorescence-based probes for interrogating major organ diseases. *Chem. Soc. Rev.* **2021,** *50*, 9391-9429.

(4) Huang, X.; Song, J.; Yung, B. C.; Huang, X.; Xiong, Y.; Chen, X., Ratiometric optical nanoprobes enable accurate molecular detection and imaging. *Chem. Soc. Rev.* **2018,** *47*, 2873-2920.

(5) Li, H.; Kim, H.; Xu, F.; Han, J.; Yao, Q.; Wang, J.; Pu, K.; Peng, X.; Yoon, J., Activity-based NIR fluorescent probes based on the versatile hemicyanine scaffold: design strategy, biomedical applications, and outlook. *Chem. Soc. Rev.* **2022,** *51*, 1795-1835.

(6) Zhang, Y.; Zhang, G.; Zeng, Z.; Pu, K., Activatable molecular probes for fluorescence-guided surgery, endoscopy and tissue biopsy. *Chem. Soc. Rev.* **2022,** *51*, 566-593.

(7) Scott, J. I.; Mendive-Tapia, L.; Gordon, D.; Barth, N. D.; Thompson, E. J.; Cheng, Z.; Taggart, D.; Kitamura, T.; Bravo-Blas, A.; Roberts, E. W.; Juarez-Jimenez, J.; Michel, J.; Piet, B.; de Vries, I. J.; Verdoes, M.; Dawson, J.; Carragher, N. O.; Connor, R. A. O.; Akram, A. R.; Frame, M.; Serrels, A.; Vendrell, M., A fluorogenic probe for granzyme B enables in-biopsy evaluation and screening of response to anticancer immunotherapies. *Nat. Commun.* **2022,** *13*, 2366.

(8) Cheng, Z.; Thompson, E. J.; Mendive-Tapia, L.; Scott, J. I.; Benson, S.; Kitamura, T.; Senan-Salinas, A.; Samarakoon, Y.; Roberts, E. W.; Arias, M. A.; Pardo, J.; Galvez, E. M.; Vendrell, M., Fluorogenic Granzyme A Substrates Enable Real-Time Imaging of Adaptive Immune Cell Activity. *Angew. Chem. Int. Ed. Engl.* **2023,** *62*, e202216142.

(9) Wu, L.; Huang, J.; Pu, K.; James, T. D., Dual-locked spectroscopic probes for sensing and therapy. *Nat. Rev. Chem.* **2021,** *5*, 406-421.

(10) Kolanowski, J. L.; Liu, F.; New, E. J., Fluorescent probes for the simultaneous detection of multiple analytes in biology. *Chem. Soc. Rev.* **2018,** *47*, 195-208.

(11) Liu, Y.; Teng, L.; Xu, C.; Liu, H. W.; Xu, S.; Guo, H.; Yuan, L.; Zhang, X. B., A "Double-Locked" and enzyme-activated molecular probe for accurate bioimaging and hepatopathy differentiation. *Chem. Sci.* **2019,** *10*, 10931-10936.

(12) Chen, M.; Wang, C.; Ding, Z.; Wang, H.; Wang, Y.; Liu, Z., A Molecular Logic Gate for Developing "AND" Logic Probes and the Application in Hepatopathy Differentiation. *ACS. Cent. Sci.* **2022,** *8*, 837-844.

(13) Widen, J. C.; Tholen, M.; Yim, J. J.; Antaris, A.; Casey, K. M.; Rogalla, S.; Klaassen, A.; Sorger, J.; Bogyo, M., AND-gate contrast agents for enhanced fluorescence-guided surgery. *Nat. Biomed. Eng.* **2021,** *5*, 264-277.

(14) Liu, C.; Zhang, R.; Zhang, W.; Liu, J.; Wang, Y. L.; Du, Z.; Song, B.; Xu, Z. P.; Yuan, J., "Dual-Key-and-Lock" Ruthenium Complex Probe for Lysosomal Formaldehyde in Cancer Cells and Tumors. *J. Am. Chem. Soc.* **2019,** *141*, 8462-8472.

(15) Tam, L. K. B.; Chu, J. C. H.; He, L.; Yang, C.; Han, K. C.; Cheung, P. C. K.; Ng, D. K. P.; Lo, P. C., Enzyme-Responsive Double-Locked Photodynamic Molecular Beacon for Targeted Photodynamic Anticancer Therapy. *J. Am. Chem. Soc.* **2023,** *145*, 7361-7375.

(16) Xiao, M.; Sun, W.; Fan, J.; Cao, J.; Li, Y.; Shao, K.; Li, M.; Li, X.; Kang, Y.; Zhang, W.; Long, S.; Du, J.; Peng, X., Aminopeptidase-N-activated Theranostic Prodrug for NIR Tracking of Local Tumor Chemotherapy. *Adv. Funct. Mater.* **2018,** *28*, 1805128.

(17) Fang, B.; Shen, Y.; Peng, B.; Bai, H.; Wang, L.; Zhang, J.; Hu, W.; Fu, L.; Zhang, W.; Li, L.; Huang, W., Small-Molecule Quenchers for Forster Resonance Energy Transfer: Structure, Mechanism, and Applications. *Angew. Chem. Int. Ed. Engl.* **2022,** *61*, e202207188.

(18) Muellers, S. N.; Tararina, M. A.; Kuzmanovic, U.; Galagan, J. E.; Allen, K. N., Structural Insights into the Substrate Range of a Bacterial Monoamine Oxidase. *Biochemistry* **2023,** *62*, 851-862.

(19) Huang, J.; Jiang, Y.; Li, J.; He, S.; Huang, J.; Pu, K., A Renal-Clearable Macromolecular Reporter for Near-Infrared Fluorescence Imaging of Bladder Cancer. *Angew. Chem. Int. Ed. Engl.* **2020,** *59*, 4415-4420.

(20) Li, H.; Yao, Q.; Sun, W.; Shao, K.; Lu, Y.; Chung, J.; Kim, D.; Fan, J.; Long, S.; Du, J.; Li, Y.; Wang, J.; Yoon, J.; Peng, X., Aminopeptidase N Activatable Fluorescent Probe for Tracking Metastatic Cancer and Image-Guided Surgery via in Situ Spraying. *J. Am. Chem. Soc.* **2020,** *142*, 6381-6389.

(21) Wang, X.; He, S.; Cheng, P.; Pu, K., A Dual-Locked Tandem Fluorescent Probe for Imaging of Pyroptosis in Cancer Chemo-Immunotherapy. *Adv. Mater.* **2023,** *35*, e2206510.

(22) He, S.; Cheng, P.; Pu, K., Activatable near-infrared probes for the detection of specific populations of tumour-infiltrating leukocytes in vivo and in urine. *Nat. Biomed. Eng.* **2023,** *7*, 281-297.

(23) J, I. Scott.; S, Gutkin; O, Green; E, J. Thompson.; T, Kitamura; D, Shabat; M, Vendrell., A Functional Chemiluminescent Probe for in Vivo Imaging of Natural Killer Cell Activity Against Tumours. *Angew. Chem. Int. Ed.* **2021**, *60*, 5699.

(24) Cheng, P.; He, S.; Zhang, C.; Liu, J.; Pu, K., A Tandem-Locked Fluorescent NETosis Reporter for the Prognosis Assessment of Cancer Immunotherapy. *Angew. Chem. Int. Ed. Engl.* **2023,** *62*, e202301625.

(25) Bertolini, M.; Wong, M. S.; Mendive-Tapia, L.; Vendrell, M., Smart probes for optical imaging of T cells and screening of anticancer immunotherapies. *Chem. Soc. Rev.* **2023,** *52*, 5352-5372.

(26) Gentles, A. J.; Newman, A. M.; Liu, C. L.; Bratman, S. V.; Feng, W.; Kim, D.; Nair, V. S.; Xu, Y.; Khuong, A.; Hoang, C. D.; Diehn, M.; West, R. B.; Plevritis, S. K.; Alizadeh, A. A., The prognostic landscape of genes and infiltrating immune cells across human cancers. *Nat. Med.* **2015,** *21*, 938-945.

(27) Bruni, D.; Angell, H. K.; Galon, J., The immune contexture and Immunoscore in cancer prognosis and therapeutic efficacy. *Nat. Rev. Cancer.* **2020,** *20*, 662-680.

(28) Kolkhir, P.; Elieh-Ali-Komi, D.; Metz, M.; Siebenhaar, F.; Maurer, M., Understanding human mast cells: lesson from therapies for allergic and non-allergic diseases. *Nat. Rev. Immunol.* **2022,** *22*, 294-308.

(29) Li, J.; Peng, G.; Zhu, K.; Jie, X.; Xu, Y.; Rao, X.; Xu, Y.; Chen, Y.; Xing, B.; Wu, G.; Shi, L., PD-1(+) mast cell enhanced by PD-1 blocking therapy associated with resistance to immunotherapy. *Cancer Immunol. Immunother.* **2023,** *72*, 633-645.

(30) Somasundaram, R.; Connelly, T.; Choi, R.; Choi, H.; Samarkina, A.; Li, L.; Gregorio, E.; Chen, Y.; Thakur, R.; Abdel-Mohsen, M.; Beqiri, M.; Kiernan, M.; Perego, M.; Wang, F.; Xiao, M.; Brafford, P.; Yang, X.; Xu, X.; Secreto, A.; Danet-Desnoyers, G.; Traum, D.; Kaestner, K. H.; Huang, A. C.; Hristova, D.; Wang, J.; Fukunaga-Kalabis, M.; Krepler, C.; Ping-Chen, F.; Zhou, X.; Gutierrez, A.; Rebecca, V. W.; Vonteddu, P.; Dotiwala, F.; Bala, S.; Majumdar, S.; Dweep, H.; Wickramasinghe, J.; Kossenkov, A. V.; Reyes-Arbujas, J.; Santiago, K.; Nguyen, T.; Griss, J.; Keeney, F.; Hayden, J.; Gavin, B. J.; Weiner, D.; Montaner, L. J.; Liu, Q.; Peiffer, L.; Becker, J.; Burton, E. M.; Davies, M. A.; Tetzlaff, M. T.; Muthumani, K.; Wargo, J. A.; Gabrilovich, D.; Herlyn, M., Tumor-infiltrating mast cells are associated with resistance to anti-PD-1 therapy. *Nat. Commun.* **2021,** *12*, 346.

(31) Komi, D. E. A.; Redegeld, F. A., Role of Mast Cells in Shaping the Tumor Microenvironment. *Clin. Rev. Allergy Immunol.* **2020,** *58*, 313-325.

(32) Marshall, J. S., Mast-cell responses to pathogens. *Nat. Rev. Immunol.* **2004,** *4*, 787-799.

(33) Dwyer, D., Barrett, N., Austen, K. *et al.* Expression profiling of constitutive mast cells reveals a unique identity within the immune system. *Nat Immunol*. **2016,** *17*, 878–887.

(34) Wernersson, S.; Pejler, G., Mast cell secretory granules: armed for battle. *Nat. Rev. Immunol.* **2014,** *14*, 478-494.

(35) Huang, C.; Wong, G. W.; Ghildyal, N.; Gurish, M. F.; Sali, A.; Matsumoto, R.; Qiu, W. T.; Stevens, R. L., The tryptase, mouse mast cell protease 7, exhibits anticoagulant activity in vivo and in vitro due to its ability to degrade fibrinogen in the presence of the diverse array of protease inhibitors in plasma. *J. Biol. Chem.* **1997,** *272*, 31885-31893.

(36) Karlson, U.; Pejler, G.; Tomasini-Johansson, B.; Hellman, L., Extended substrate specificity of rat mast cell protease 5, a rodent alpha-chymase with elastase-like primary specificity. *J. Biol. Chem.* **2003,** *278*, 39625-39631.

(37) Zheng, X.; Wang, X.; Mao, H.; Wu, W.; Liu, B.; Jiang, X., Hypoxia-specific ultrasensitive detection of tumours and cancer cells in vivo. *Nat. Commun.* **2015,** *6*, 5834.

(38) Niu, H.; Liu, J.; O'Connor, H. M.; Gunnlaugsson, T.; James, T. D.; Zhang, H., Photoinduced electron transfer (PeT) based fluorescent probes for cellular imaging and disease therapy. *Chem. Soc. Rev.* **2023,** *52*, 2322-2357.

(39) Benedé, S., Cody, E., Agashe, C., Berin, MC. Immune Characterization of Bone Marrow-Derived Models of Mucosal and Connective Tissue Mast Cells. Allergy *Asthma Immunol Res.* **2018**, 10, 268-277.

(40) Kunori, Y.; Koizumi, M.; Masegi, T.; Kasai, H.; Kawabata, H.; Yamazaki, Y.; Fukamizu, A., Rodent alpha-chymases are elastase-like proteases. *Eur. J. Biochem.* **2002**, *269*, 5921-5930

(41) Samoszuk, M.; Corwin, M. A., Mast cell inhibitor cromolyn increases blood clotting and hypoxia in murine breast cancer. *Int. J. Cancer* **2003,** *107*, 159-163.

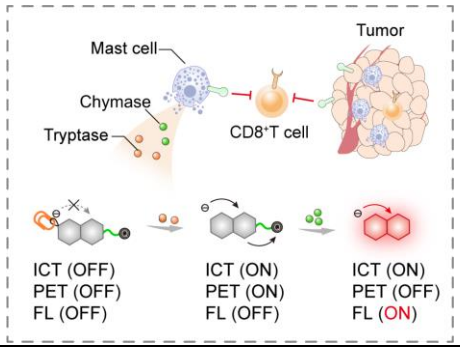
Mast cell
Chymase
Tryptase
CD8⁺T cell
Tumor
ICT (OFF)
PET (OFF)
FL (OFF)
ICT (ON)
PET (ON)
FL (OFF)
ICT (ON)
PET (OFF)
FL (ON)